Supplementary Data

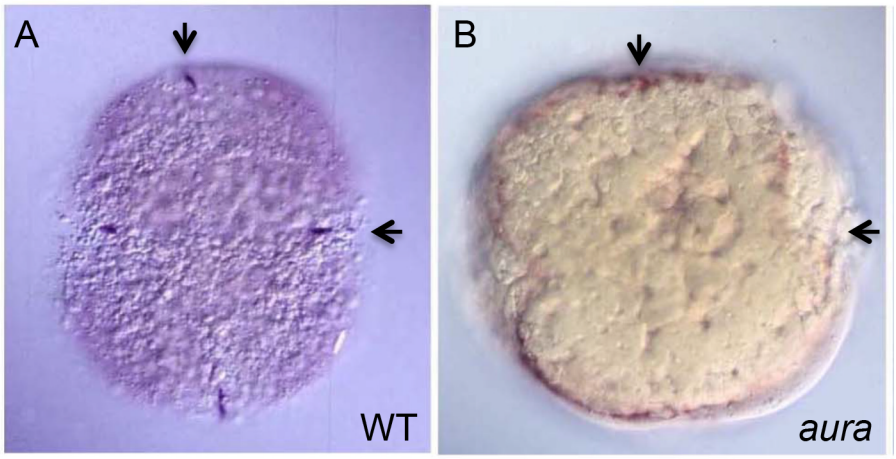

Figure S1: *vasa* RNA localization in *aura* mutant embryos. 4-cell stage embryos showing normal RNA furrow localization in wild-type (A) and reduced furrow localization and increase marginal enrichment in *aura* mutants (B). *vasa* RNA visualized as in Fig. 2A,B but using DAB (blue) visible substrate. Arrows show cleavage planes.

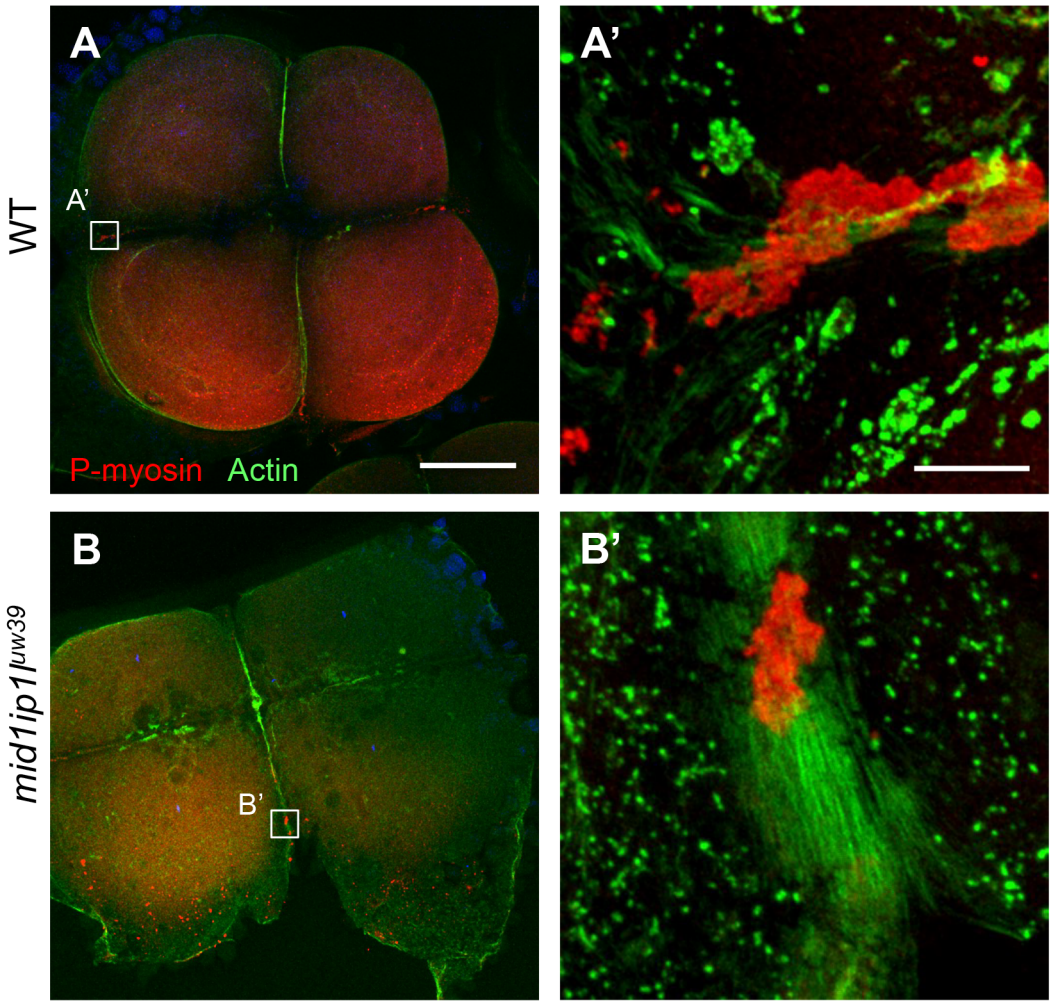

Figure S2: Maternal-effect germ plasm segregation defect in mutants for *mid1ip1l*^{uw39}. Localization of RNPs (using an anti-P-myosin antibody) and F-actin in wild-type (A, A') and embryos from females homozygous for the *mid1ip1l*^{uw39} alllele (B,B'). Scale: 100 µM A-D (bar in A), 10 µM A',B' (bar in A').

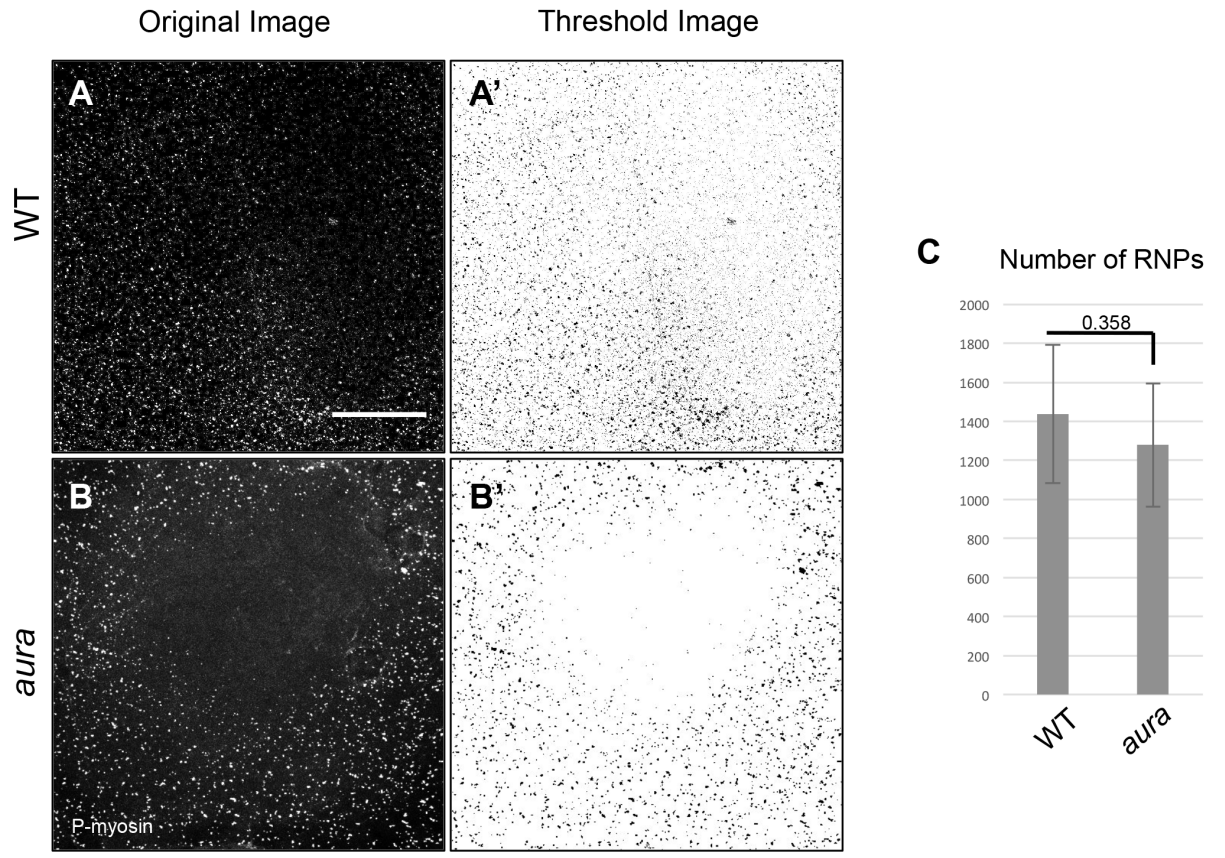

Figure S3: *aura* mutant embryos exhibit a similar initial number of cortical germ plasm RNPs. Wild-type and *aura* mutant embryos fixed at 12 mpf show a similar number of RNPs. (A.B) Labeling of RNP with anti-P-myosin. (A',B') Reversed grayscale for improved visualization. The RNP zone in the center of the blastodisc is likely the incipient zone of RNP clearing, which our observations suggest moves outward faster in *aura* mutants than in wild-type. (C) Quantification of the number of spots in image fields using automated particle counting (FIJI) shows no statistically significant difference between wild-type and mutant embryos (8 embryos each). Scale: 100 μM.

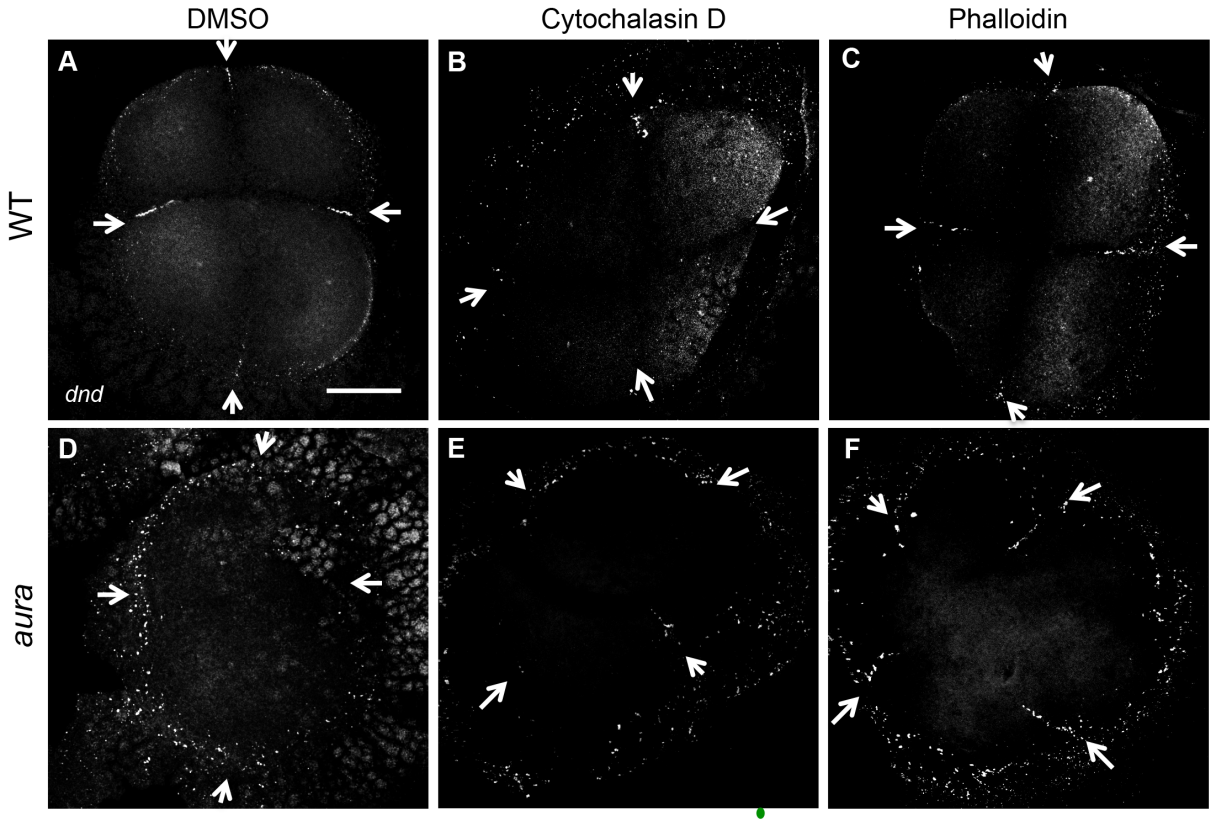

Figure S4: Effects of cytoskeletal inhibitors on germ plasm RNP furrow recruitment.
Fluorescent in situ hybridization to visualize *dnd* RNA localization. Scale: 100 µM A-F (bar in A)

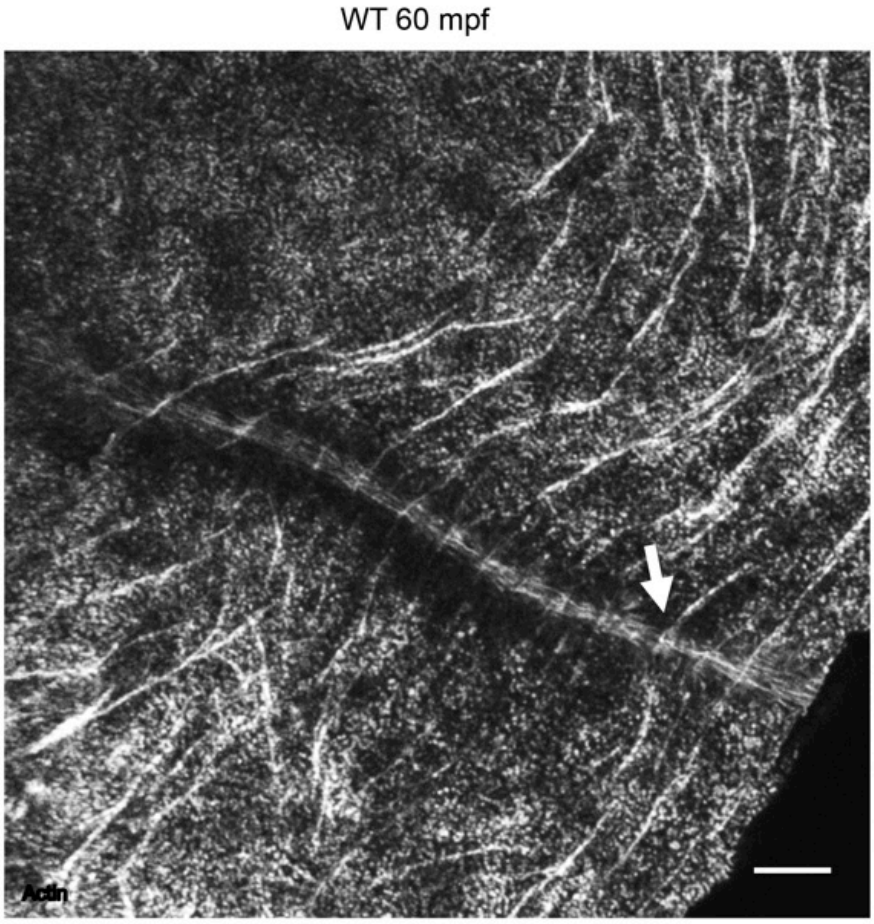

Figure S5: F-actin cortical trenches converge with F-actin furrow indentations. Overview of a wild-type embryo labeled for F-actin, showing that many circumferential F-actin arcs, which correspond to cortical trenches (Fig. 7A), connect to F-actin enrichments at the furrow (Fig. 7B), which correspond to furrow indentations.

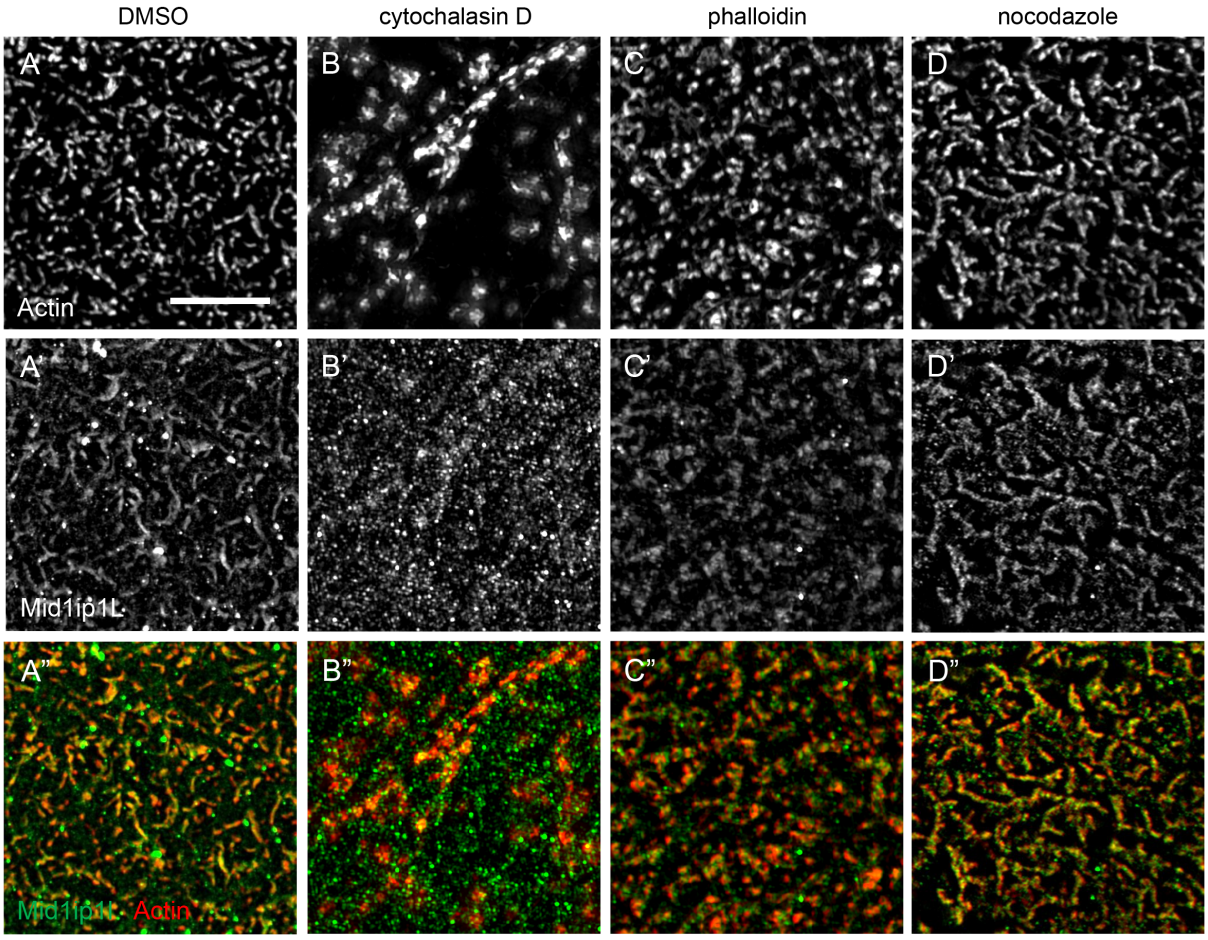

Figure S6: Mid1ip1L protein localization depends on F-actin, but not microtubules. SIM images showing localization of Mid1ip1l with respect to F-actin in the presence of cytoskeletal inhibitors. Both actin inhibition (B-B") and stabilization (C-C") lead to a reduction in colocalization. Colocalization appears unaffected by microtubule inhibition (D-D"). Scale: 5 μM A-H (bar in A).

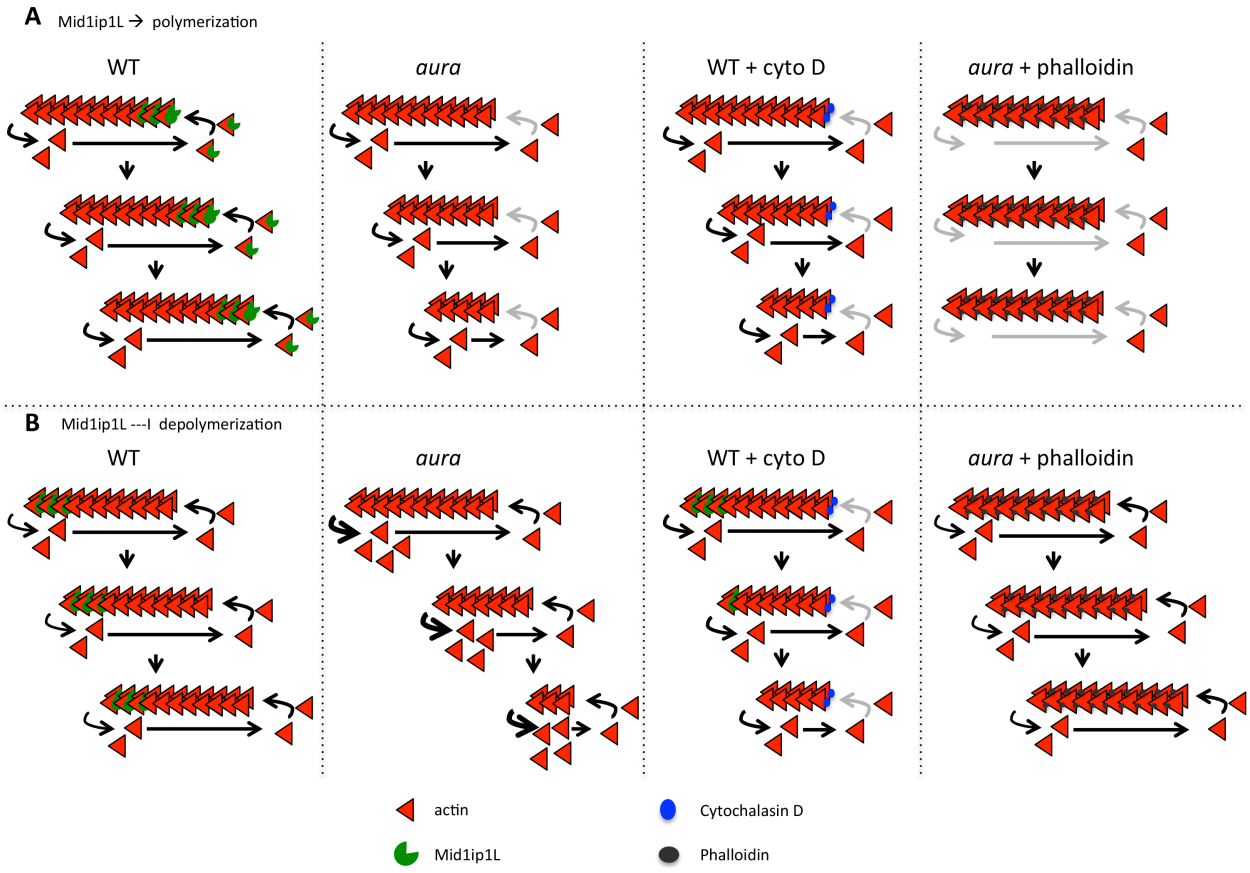

Figure S7: Potential mechanisms by which Mid1ip1L may regulate actin dynamics, and relation to inhibitor effects. Models based on the observed binding of Mid1ip1L to one end of short F-actin (Fig. 9), and effects of the cytochalasin D and phalloidin on the *aura* phenotype. A) Mid1ip1L promotes F-actin polymerization at the site of actin monomer addition (plus ends), so that reduced function results in decreased polymerization. B) Mid1ip1L downregulates the rate of F-actin depolymerization at the minus ends, so that the reduced function results in increased F-actin depolymerization. In both models, both *aura* mutants and cytochalasin D-treated wild-type embryos exhibit F-actin loss. In both models, stabilization of F-actin with phalloidin reduces the rate F-actin loss, allowing for the formation of short F-actin and partially rescuing the phenotype. Plus (barbed) end are shown on right and minus (pointed) ends on left, with F-actin treadmilling indicated by growth to the right from top (early in sequence) to bottom (later in sequence).

Table S1. Primers used for end-point genotyping.

Primer Name	5'-> 3'	Use
mid1ip1L Forward	TATCACCTCCACGGACTCTT	genotyping
mid1ip1L Reverse	CCGCCGATTTCTCTCTTGT	genotyping
mid1ip1L MUT Probe	/56FAM/TGT +C+C+T +AA+C +TAA C/3IABkFQ/	genotyping
mid1ipL WT Probe	/5HEX/TGT +C+C+A +AA+C T+AA CA/3IABkFQ/	genotyping

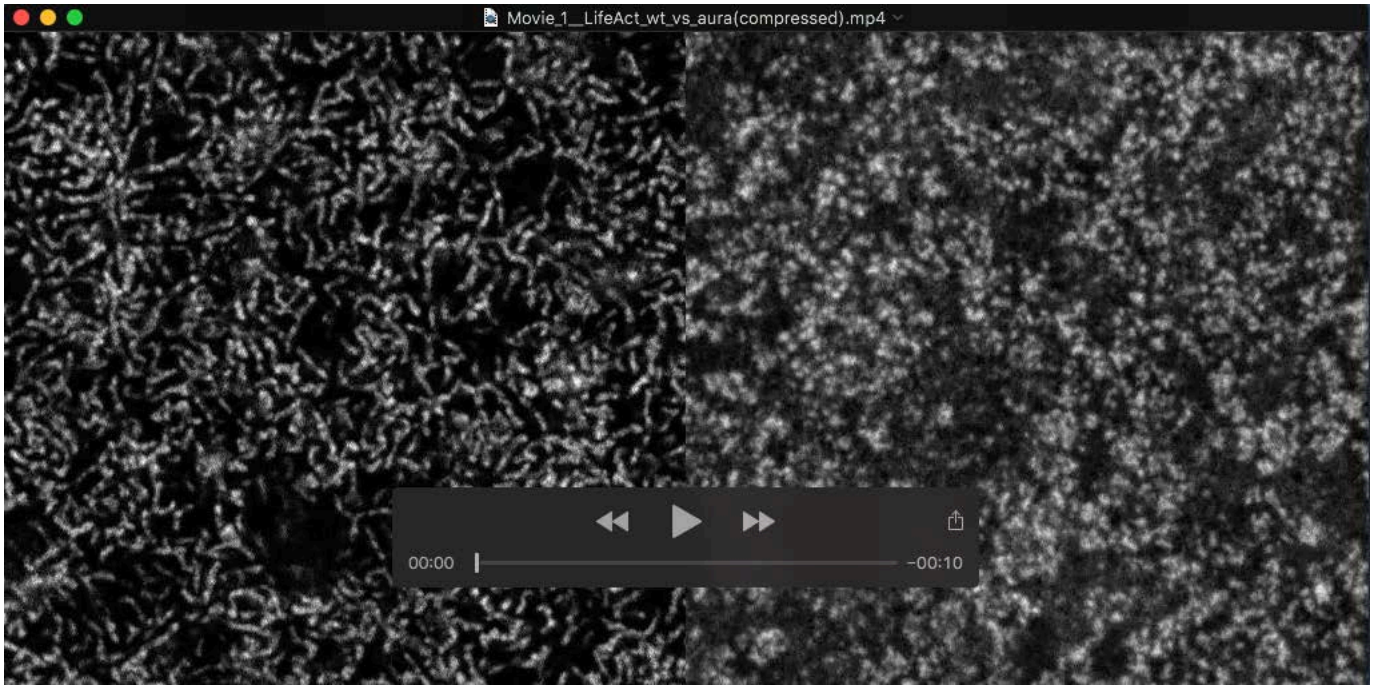

Movie 1. Cortical F-actin in live embryos: wild-type vs *aura* mutants. Left: In wild-type, cortical F-actin exhibits dynamic cyclical changes and local undulations. Movie corresponds to still data in Fig. 6A. Representative movie of 10 trials. Right: In *aura* mutants, cortical F-actin appears static and exhibits an aberrant reorganization. Movie corresponds to still data in Fig. 6B. Representative movie of 10 trials. In both movies, F-actin is detected by the Life Act transgene, with images at 200x magnification, corresponding to scale bar in Fig. 6.

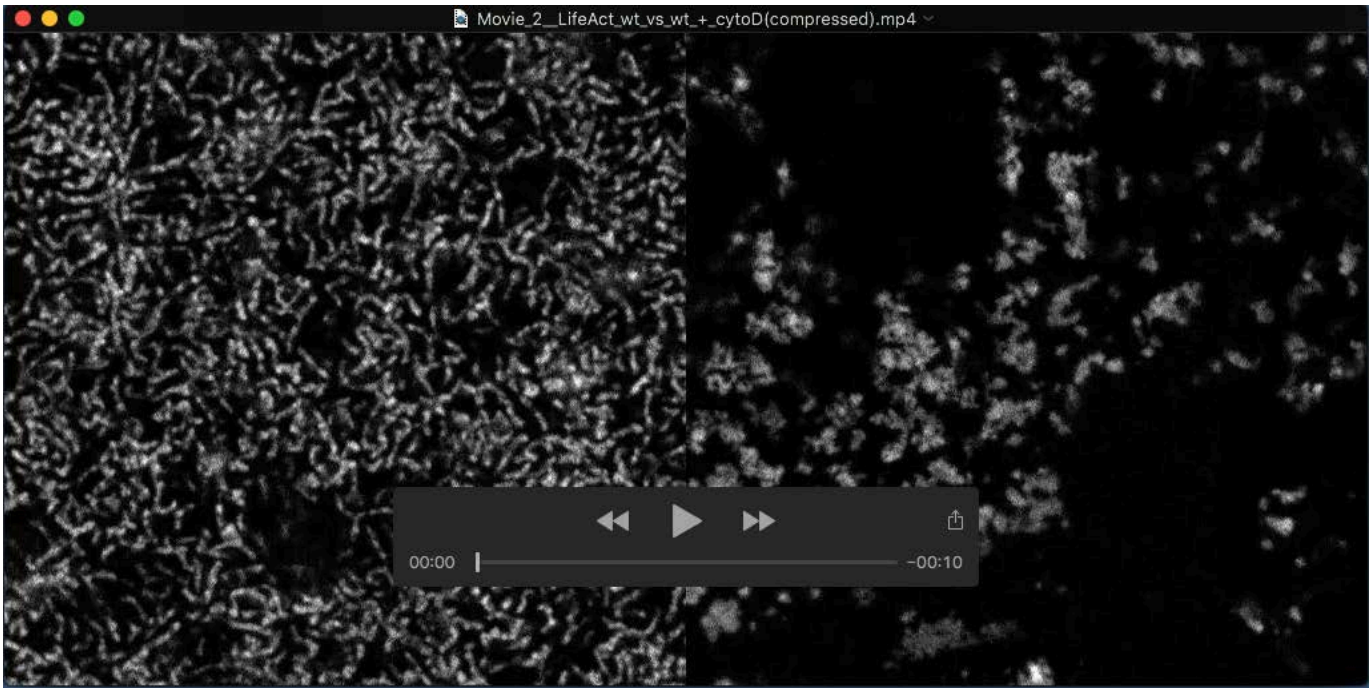

Movie 2. Cortical F-actin in live embryos: effect of cytochalasin D in wild-type. Left: cortical F-actin in wild-type, as in Movie 1 (left) and corresponding to still data in Fig. 6A. Right: F-actin cortex appears degraded, consistent with F-actin depolymerization. Representative movie of 3 trials. In both movies, F-actin is detected by the Life Act transgene, with images at 200x magnification, corresponding to scale bar in Fig. 6.

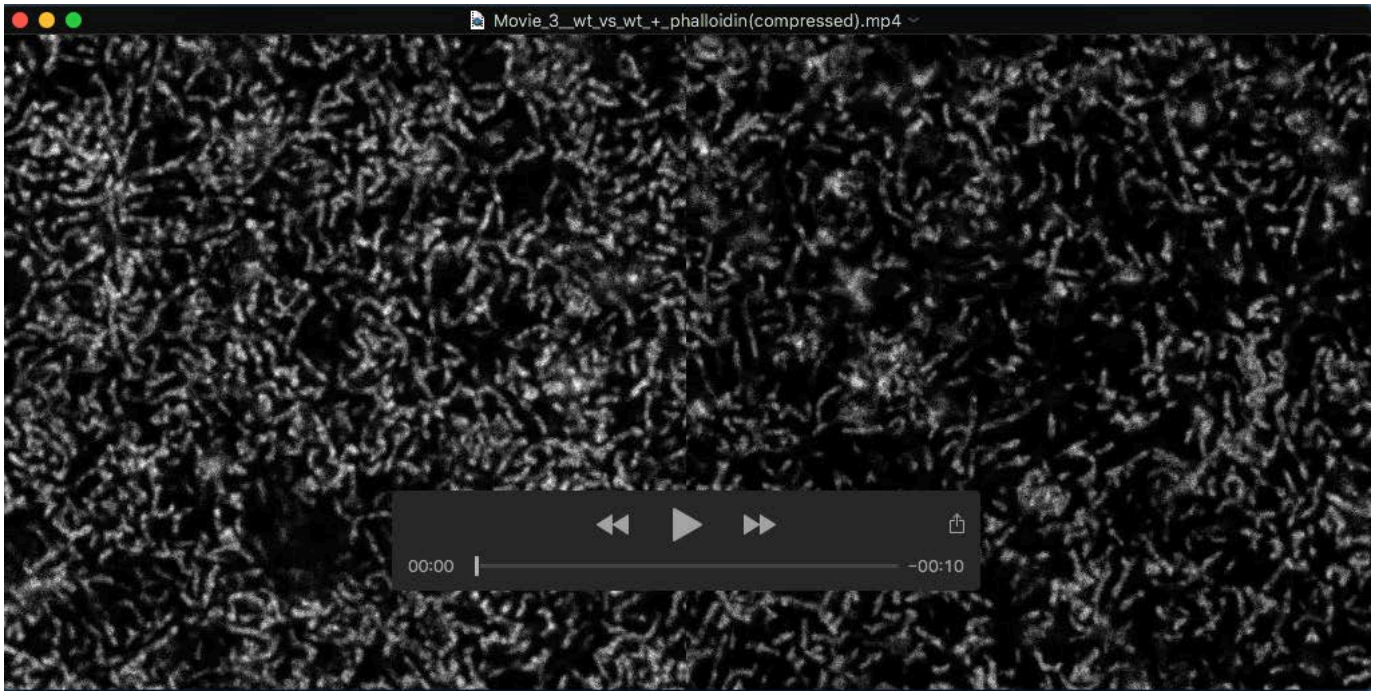

Movie 3. Cortical F-actin in live embryos: effect of phalloidin in wild-type. Left: cortical F-actin in wild-type, as in Movie 1 (left) and corresponding to still data in Fig. 6A. Right: F-actin dynamic movements are present. Representative movie of 2 trials. Apparently wider oscillations of the cortex compared to untreated embryos are observed in both movies. In both movies, F-actin is detected by the Life Act transgene, with images at 200x magnification, corresponding to scale bar in Fig. 6.

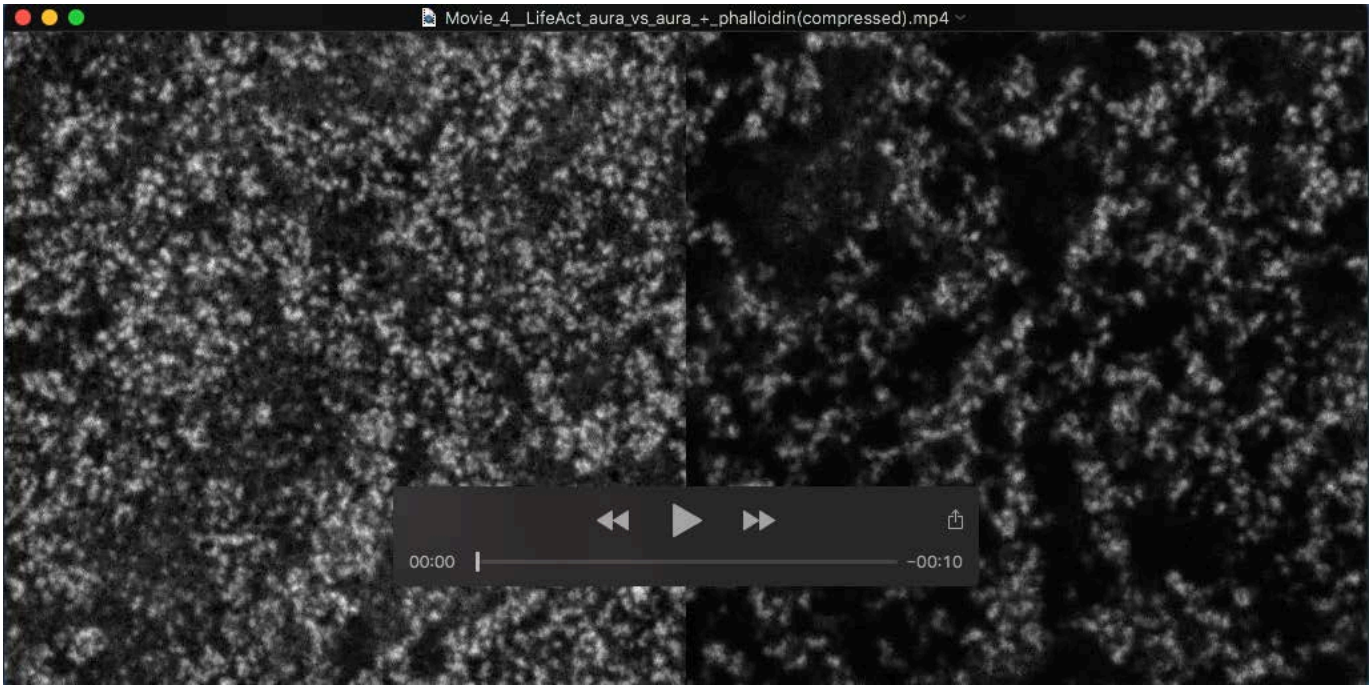

Movie 4. Cortical F-actin in live embryos: partial rescue of F-actin dynamics in *aura* mutants by phalloidin treatment. Left: cortical F-actin in *aura* mutants, as in Movie 1 (right) and corresponding to still data in Fig. 6B. F-actin dynamics defects characteristic or *aura* mutants are partially restored, as manifested by local cortical contractions and expansions. Representative movie of 3 trials. In both movies, F-actin is detected by the Life Act transgene, with images at 200x magnification, corresponding to scale bar in Fig. 6.